ESTIMATION OF THE UNCERTAINTIES AND ERRORS OF THE TECHNIQUES USED TO MEASURE MULTI-LAYER ANISOTROPIC STRUCTURES DISTORTIONS

Cesar BANU [1], Mihai BUGARU [2, *]

In the field of mechanical engineering, measurements are used to determine physical properties such as deformation, stress, velocity, temperature, or applied force. Each of these measurements requires appropriate equipment and specific methods for uncertainty analysis, as small slight variations in measurement results can have significant implications for the design and reliability of mechanical components. For example, in the study of laminated composite structures, distortions resulting from mechanical or thermal loads must be measured accurately, as these values directly influence the material's mechanical performance and durability. When reporting the result of a measurement of a physical quantity, it is mandatory to provide a quantitative indication of the quality of the result, so that those who use it can assess its reliability. Without such an indication, measurement results cannot be compared with one another or with reference values specified in a specification or standard. Therefore, a procedure is required that is easy to implement, easy to understand, and widely accepted for characterizing the quality of a measurement result—namely, for evaluating and expressing its uncertainty. This work presents a robust method for assessing CMM measuring uncertainty. The article contains the calculated uncertainty results and the comparison with the CMM equipment calibration certificate.

Keywords: measuring error; measuring uncertainty; distortion; CMM

1. Introduction

The advancements in technology and science outlined in this article were part of the project titled "Evaluation of Composite Laminate Distortion through an Integrated Numerical-Experimental Approach – ELADINE" [**1**]. This initiative functioned as a supporting activity (CfP) for the OPTICOMS project [**2**], which was executed under the European Clean Sky 2 program. The primary aim of ELADINE was to develop an innovative numerical tool for predicting the spring-in effect in the primary structural components of a regional transport aircraft wing. This methodology was based on the development and validation of numerical simulations using experimental data from polymerization. To calibrate

* Corresponding author
[1] Eng., National Institute for Aerospace Research and Development – INCAS, Bucharest, Romania, banu.cesar@incas.ro
[2] Prof., Dept. of Mechanics, National University for Sciences and Technology POLITEHNICA Bucharest, Romania, skmbugaru@yahoo.com

and validate the simulation numerical tool, the experimental program included extended measurements on both simple coupons and complex test specimens. The process commenced with tests on simple flat specimens and was later expanded to include C-shaped specimens, small-scale wing section demonstrators, and ultimately culminated in a full-scale 7-meter wing demonstrator.

The uncertainty associated with a measurement outcome indicates the absence of precise knowledge regarding the value of the quantity being measured [**4,5**]. Even after adjustments for acknowledged systematic influences, the result of a measurement approximates the actual value of the measured quantity, due to uncertainties stemming from random variations and the incomplete correction of systematic effects. [**4-8**].

The measurement uncertainty is often estimated using the standard deviation of repeated measurements [**5, 9**]:

$$u = \sqrt{\frac{\sum \left(x_i - \bar{x} \right)^2}{n-1}} \tag{1}$$

In which x_i are the individual measurements, $\bar{x}$ is the mean value, and $\boldsymbol{i}$ is the number of measurements.

2. Evaluation of deviations and uncertainties for the geometry measurements of test specimens using a Coordinate Measuring Machine (CMM)

Coordinate Measuring Machines (CMMs) are widely used in industry for verifying the accuracy of mechanical components. To ensure accurate and repeatable measurements, proper calibration of the CMM is essential. This subsection presents calibration techniques, the required steps, and relevant application examples. To estimate the measurement uncertainty due to workpiece temperature, ideally, the entire measurement process could be mathematically modelled, including all relevant parameters that may influence the measurement, as indicated in Equation (2)[**3**]

$$y = f\left(x_1, x_2, \ldots x_N \right) \tag{2}$$

in which measured value *Y* depends on *N* input quantities.

A model for measurement uncertainty can then be developed using the law of propagation of uncertainty, i.e., Equation (3), and by estimating the variances and covariances of the individual uncertainty components [**3**]

$$u_y = \sqrt{\left(\frac{\partial y}{\partial x_1} u_{x_1} \right)^2 + \left(\frac{\partial y}{\partial x_2} u_{x_2} \right)^2 + \ldots} \tag{3}$$

in which u_{x_i} are the uncertainties of the individual measurements.

Ideally, we would aim to develop a comprehensive mathematical model of the measurement process that would describe all possible measurements performed using a Coordinate Measuring Machine (CMM). Such a model would encompass all factors that influence the accuracy of the measurement result. By applying the law of propagation of uncertainty, one could obtain the combined standard uncertainty of a measurement performed with a CMM.

It is essential to note that for correlated input variables, the uncertainty propagation must also account for the corresponding covariance terms.

Unfortunately, a detailed and precise mathematical model of CMM-based measurements is currently unavailable. Since it is not yet feasible to determine rigorously—a priori—the uncertainty for most measurements a CMM can perform, various national and industrial standards [**9–12**] have adopted an alternative approach: characterizing CMM performance through a series of well-defined and documented tests, performed on standards with extremely low form error and elementary geometries (e.g., disks, spheres, parallel planes, etc.).

Determining the combined standard uncertainty for an actual CMM measurement is a complex task that involves several aspects. To clarify the issue, we distinguish between several different sources of error, namely: "operational error," "sampling strategy effects," and "algorithmic error."

(From a technical standpoint, it would be more accurate to replace "algorithmic error" with "mathematical modelling error," but we consider the former term to be more familiar to regular CMM users.)

For the estimation of shape distortion in the fabricated specimens, a Hexagon GLOBAL Advantage 20.40.18 coordinate measuring machine was used, equipped with a 2 mm diameter probe, to compare results with the response of Fiber Bragg Grating (FBG) optic sensors and calibrate them. To compare different measurements taken on different days, the test specimen (Figure 1) had to be positioned in the same manner each time. Therefore, it was placed on a support fixture—the master mold used for manufacturing the test specimen molds (see the green surface in Figure 2).

The CMM equipment calibration results are presented in Table 1:

Table 1 **[12]**

Reference measurement (mm)	X Axis (μm)	Reference measurement (mm)	Y Axis (μm)	Reference measurement (mm)	Z Axis (μm)
380	-1,6	700	1,2	320	-1,4
760	-1,1	1400	-0,1	640	-1,5
1140	-0,6	2100	2,4	960	-1,5
1520	-0,7	2800	1,4	1280	-2,2
1900	-1,0	3500	-1,3	1600	-2,0

Excerpts from the calibration certificate of the measurement equipment [**13**]:

- Calibration results of the probe P (µm)
- Maximum difference of the 25 polar radii: P = 0.8 µm
- Measurement uncertainty: U = 0.5 µm

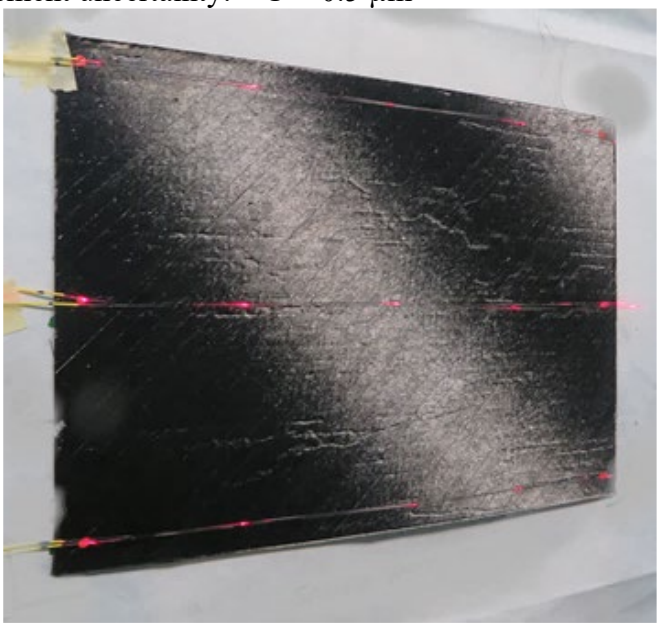

Fig. 1. Photograph of a Skin coupon with 3 arrays of 5 FBG sensors for strain measurement (red lighted spots are the places where the FBG sensors are in the fiber optics) [**14**]

Fig. 2. Composite skin specimen placed on the support fixture (master tool) of the 3D CMM for shape distortion evaluation, with FBG sensors connected [**14**]

To evaluate the changes in the Z-coordinate during the first 9 days after manufacturing, a measurement scheme with 80 points uniformly distributed across the specimen geometry was used – Figure 3.

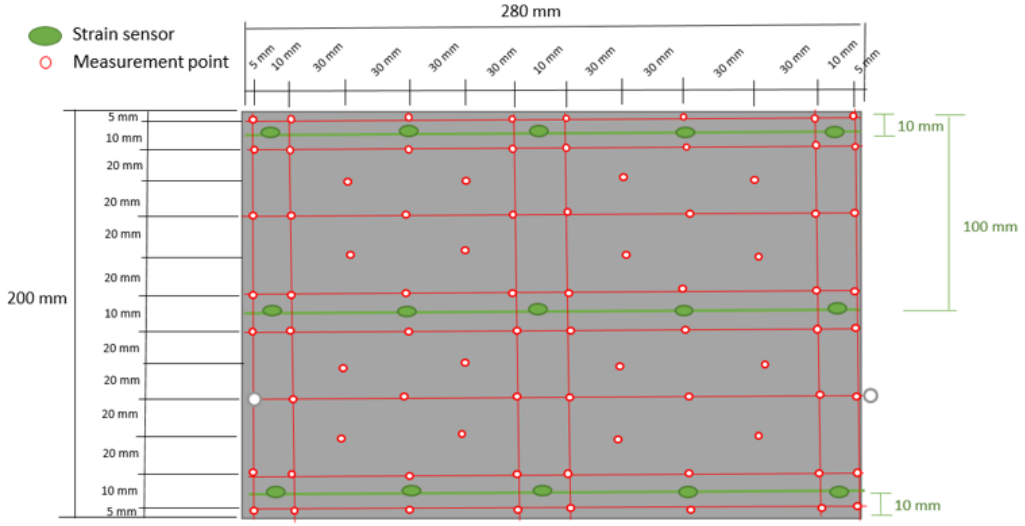

Fig. 3. Skin coupon coordinate points distribution for shape distortions using 3D CMM [**14**]

The measured values are listed in Table 2. Based on the measurement results from the X, Y, and Z columns, we calculated the ***r*** column of Table 2, using the following relation [**14**]:

$$r = \sqrt{X^2 + Y^2 + Z^2}\,(mm) \tag{4}$$

Starting from relation 4, we calculated the error for each of the X, Y, and Z directions as follows [**13**]:

$$\Delta_{x,y,z} = \left(4.5 + 1 \cdot \frac{L}{250}\right)(\mu m) \tag{5}$$

where L is the measured distance.

The value of the absolute error is calculated using the relation [**14**]:

$$\Delta_{abs} = \sqrt{\Delta_X^2 + \Delta_Y^2 + \Delta_Z^2}\,(\mu m) \tag{6}$$

Where Δ_X, Δ_Y, Δ_Z are the values of the measurement error corresponding to the three axes.

Table 2 **[14]**

	X (mm)	Y (mm)	Z (mm)	r (mm)
			07/09/2020	
PNT001	5.0	5.0	5.175	8.762
PNT002	15.0	5.0	6.105	16.949
PNT003	75.0	5.0	10.251	75.862
PNT004	135.0	5.0	11.833	135.610
PNT005	145.0	5.0	11.84	145.568
PNT006	205.0	5.0	10.334	205.321
PNT007	265.0	5.0	6.145	265.118
PNT008	275.0	5.0	5.191	275.094
PNT009	275.0	15.0	5.2	275.458
PNT010	265.0	15.0	6.16	265.496
PNT011	205.0	15.0	10.36	205.809
PNT012	145.0	15.0	11.842	146.254
PNT013	135.0	15.0	11.855	136.347
PNT014	75.0	15.0	10.275	77.172
PNT015	15.0	15.0	6.1	22.073
PNT016	5.0	15.0	5.155	16.631
PNT017	5.0	55.0	5.15	55.466
PNT018	15.0	55.0	6.105	57.335
PNT019	45.0	35.0	8.529	57.643
PNT020	75.0	55.0	10.327	93.577
PNT022	105.0	35.0	11.434	111.269
PNT023	135.0	55.0	11.884	146.257
PNT024	145.0	55.0	11.867	155.534
PNT025	175.0	35.0	11.438	178.832
PNT026	205.0	55.0	10.341	212.502
PNT027	235.0	35.0	8.582	237.747
PNT028	265.0	55.0	6.163	270.718
PNT029	275.0	55.0	5.203	280.494
PNT030	275.0	95.0	5.161	290.993
PNT031	265.0	95.0	6.117	281.580
PNT032	235.0	75.0	8.576	246.827
PNT033	205.0	95.0	10.321	226.178
PNT034	175.0	75.0	11.442	190.738
PNT035	145.0	95.0	11.87	173.755
PNT036	135.0	95.0	11.872	165.502
PNT037	105.0	75.0	11.448	129.542
PNT038	75.0	95.0	10.337	121.478
PNT039	45.0	75.0	8.545	87.881
PNT040	15.0	95.0	6.091	96.370
PNT041	5.0	95.0	5.128	95.270
PNT042	5.0	105.0	5.125	105.244
PNT043	15.0	105.0	6.098	106.241
PNT044	75.0	105.0	10.325	129.447
PNT045	135.0	105.0	11.842	171.436
PNT046	145.0	105.0	11.868	179.418
PNT047	205.0	105.0	10.339	230.558
PNT048	265.0	105.0	6.112	285.109
PNT049	275.0	105.0	5.154	294.409
PNT050	275.0	145.0	5.144	310.928
PNT051	265.0	145.0	6.109	302.138
PNT052	235.0	125.0	8.562	266.314
PNT053	205.0	145.0	10.344	251.311
PNT054	175.0	125.0	11.454	215.363
PNT055	145.0	145.0	11.892	205.406
PNT056	135.0	145.0	11.896	198.473
PNT057	105.0	125.0	11.438	163.648
PNT058	75.0	145.0	10.3	163.573
PNT059	45.0	125.0	8.539	133.127
PNT060	15.0	145.0	6.095	145.901
PNT061	5.0	145.0	5.124	145.177
PNT062	5.0	185.0	5.118	185.138
PNT063	15.0	185.0	6.077	185.707
PNT064	45.0	165.0	8.548	171.240
PNT065	75.0	185.0	10.324	199.891
PNT066	105.0	165.0	11.461	195.912
PNT067	135.0	185.0	11.881	229.328
PNT068	145.0	185.0	11.869	235.353
PNT069	175.0	165.0	11.459	240.793
PNT070	205.0	185.0	10.343	276.328
PNT071	235.0	165.0	8.548	287.268
PNT072	265.0	185.0	6.093	323.245
PNT073	275.0	185.0	5.118	331.476
PNT074	275.0	195.0	5.098	337.159
PNT075	265.0	195.0	6.057	329.069
PNT076	205.0	195.0	10.323	283.119
PNT077	145.0	195.0	11.879	243.292
PNT078	135.0	195.0	11.868	237.468
PNT079	75.0	195.0	10.316	209.180
PNT080	15.0	195.0	6.068	195.670
PNT081	5.0	195.0	5.072	195.130

Table 3 **[14]**

X Delta	Y Delta	Z Delta	Abs. Delta
4.52	4.52	4.52	7.83
4.56	4.52	4.52	7.85
4.8	4.52	4.54	8.01
5.04	4.52	4.55	8.16
5.08	4.52	4.55	8.18
5.32	4.52	4.54	8.33
5.56	4.52	4.52	8.47
5.6	4.52	4.52	8.50
5.6	4.56	4.52	8.52
5.56	4.56	4.52	8.50
5.32	4.56	4.54	8.35
5.08	4.56	4.55	8.20
5.04	4.56	4.55	8.18
4.8	4.56	4.54	8.03
4.56	4.56	4.52	7.88
4.52	4.56	4.52	7.85
4.52	4.72	4.52	7.95
4.56	4.72	4.52	7.97
4.68	4.64	4.53	8.00
4.8	4.72	4.54	8.12
4.92	4.64	4.55	8.15
5.04	4.72	4.55	8.27
5.08	4.72	4.55	8.29
5.2	4.64	4.55	8.32
5.32	4.72	4.54	8.44
5.44	4.64	4.53	8.47
5.56	4.72	4.52	8.58
5.6	4.72	4.52	8.61
5.6	4.88	4.52	8.70
5.56	4.88	4.52	8.67
5.44	4.8	4.53	8.56
5.32	4.88	4.54	8.53
5.2	4.8	4.55	8.41
5.08	4.88	4.55	8.38
5.04	4.88	4.55	8.36
4.92	4.8	4.55	8.24
4.8	4.88	4.54	8.21
4.68	4.8	4.53	8.09
4.56	4.88	4.52	8.07
4.52	4.88	4.52	8.04
4.52	4.92	4.52	8.07
4.56	4.92	4.52	8.09
4.8	4.92	4.54	8.24
5.04	4.92	4.55	8.38
5.08	4.92	4.55	8.41
5.32	4.92	4.54	8.55
5.56	4.92	4.52	8.69
5.6	4.92	4.52	8.72
5.6	5.08	4.52	8.81
5.56	5.08	4.52	8.79
5.44	5	4.53	8.67
5.32	5.08	4.54	8.64
5.2	5	4.55	8.53
5.08	5.08	4.55	8.50
5.04	5.08	4.55	8.48
4.92	5	4.55	8.36
4.8	5.08	4.54	8.33
4.68	5	4.53	8.21
4.56	5.08	4.52	8.19
4.52	5.08	4.52	8.17
4.52	5.24	4.52	8.27
4.56	5.24	4.52	8.29
4.68	5.16	4.53	8.31
4.8	5.24	4.54	8.43
4.92	5.16	4.55	8.46
5.04	5.24	4.55	8.58
5.08	5.24	4.55	8.60
5.2	5.16	4.55	8.62
5.32	5.24	4.54	8.74
5.44	5.16	4.53	8.76
5.56	5.24	4.52	8.88
5.6	5.24	4.52	8.90
5.6	5.28	4.52	8.93
5.56	5.28	4.52	8.90
5.32	5.28	4.54	8.76
5.08	5.28	4.55	8.62
5.04	5.28	4.55	8.60
4.8	5.28	4.54	8.46
4.56	5.28	4.52	8.32
4.52	5.28	4.52	8.29

The calculated values were included in Table 3. Based on the numerical values from Table 3, the graph showing the variation of measurement deviations as a function of the measured value is plotted, as presented in Figure 4.

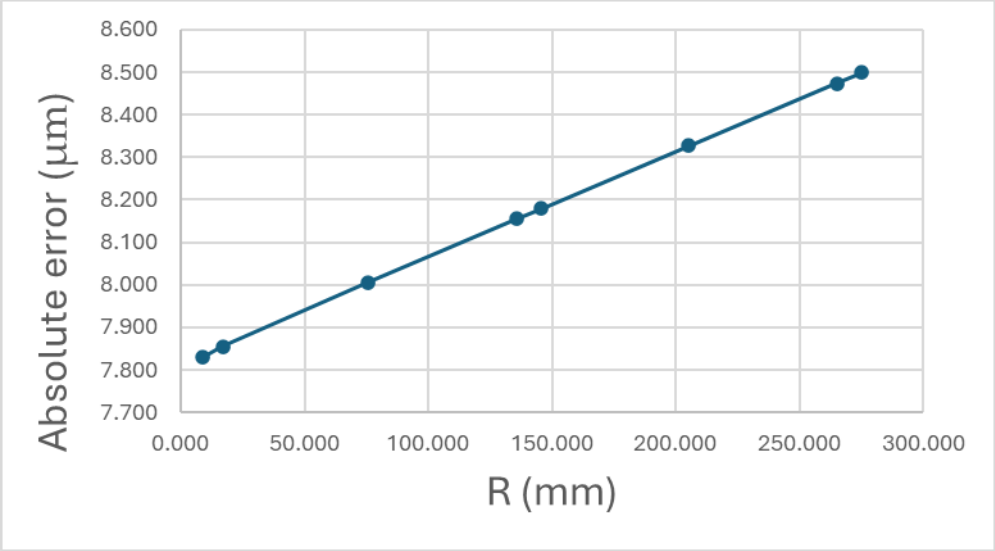

Fig. 4. Absolute error variation vs measured distance [**14**]

Table 4 **[14]**

Meas. point [No.]	[X] α angle (deg)	[X] α - 2.5° (deg)	[X] α + 2.5° (deg)	[X] Error (µm)
1	55.2067972	52.7068	57.7068	4.52
2	27.74796378	25.24796	30.24796	4.56
3	8.646831624	6.146832	11.14683	4.8
4	5.435649292	2.935649	7.935649	5.04
5	5.065324857	2.565325	7.565325	5.08
6	3.205230626	0.705231	5.705231	5.32
7	1.712349986	-0.78765	4.21235	5.56
8	1.501304155	-0.9987	4.001304	5.6
9	3.304022478	0.804022	5.804022	5.6
10	3.501616926	1.001617	6.001617	5.56
11	5.08174059	2.581741	7.581741	5.32

	4			
12	7.508335541	5.008336	10.00834	5.08
13	8.060804374	5.560804	10.5608	5.04
14	13.6269404	11.12694	16.12694	4.8
15	47.19008599	44.69009	49.69009	4.56

Meas. point [No.]	[Y] β angle (deg)	[Y] β - 2.5° (deg)	[Y] β + 2.5° (deg)	[Y] Error (µm)
1	9.635407936	7.135407936	12.13540794	4.52
2	12.71340141	10.21340141	15.21340141	4.56
3	15.04840551	12.54840551	17.54840551	4.8
4	15.33918455	12.83918455	17.83918455	5.04
5	15.36442455	12.86442455	17.86442455	5.08
6	15.46442814	12.96442814	17.96442814	5.32
7	15.51936698	13.01936698	18.01936698	5.56
8	15.51936698	13.01936698	18.01936698	5.56
9	15.52620737	13.02620737	18.02620737	5.6
10	15.16315556	12.66315556	17.66315556	5.6
11	15.14269092	12.64269092	17.64269092	5.56
12	14.97849478	12.47849478	17.47849478	5.32
13	14.68055305	12.18055305	17.18055305	5.08
14	14.60560812	12.10560812	17.10560812	5.04
15	13.75181972	11.25181972	16.25181972	4.8
Meas. point [No.]	[Z] γ angle (deg)	[Z] γ - 2.5° (deg)	[Z] γ + 2.5° (deg)	[Z] Error (µm)
1	53.8012739	51.3012739	56.3012739	4.52
2	68.8877364	66.3877364	71.3877364	4.56

	4	4	4	
3	82.2340839	79.7340839	84.7340839	4.8
4	84.99415358	82.49415358	87.49415358	5.04
5	85.3346383	82.8346383	87.8346383	5.08
6	87.11505116	84.61505116	89.61505116	5.32
7	88.67187936	86.17187936	91.17187936	5.56
8	88.91878962	86.41878962	91.41878962	5.6
9	88.91834402	86.41834402	91.41834402	5.6
10	88.67052901	86.17052901	91.17052901	5.56
11	87.11464699	84.61464699	89.61464699	5.32
12	85.35576753	82.85576753	87.85576753	5.08
13	85.01201249	82.51201249	87.51201249	5.04
14	82.34873616	79.84873616	84.84873616	4.8
15	73.95706842	71.45706842	76.45706842	4.56

Starting with the measurement data in Table 2, corresponding to the *X, Y,* and *Z* columns and the values of the computed errors listed in Table 3, the values of the α, β, and γ angles have been calculated, which correspond to all the CMM positions during the measurements. The relations 7-9 have been employed [**14**]:

$$\alpha = acos\frac{L_x}{\sqrt{L_X^2 + L_Y^2 + L_Z^2}} \tag{7}$$

$$\beta = acos\frac{L_y}{\sqrt{L_X^2 + L_Y^2 + L_Z^2}} \tag{8}$$

$$\gamma = acos\frac{L_z}{\sqrt{L_X^2 + L_Y^2 + L_Z^2}} \tag{9}$$

where L_X, L_Y, L_Z are the measured distances on the three corresponding directions.

Using the obtained values of the angles and the error values from Table 3, the data sets presented in Table 4 were compiled. Knowing the angular error of 2.5° of the CMM measuring equipment, we used the data from Table 4 to create the polar dispersion diagrams shown in Figures 5, 6, and 7 [**13**]. Analyzing the polar chart

in Figure 5, it is observed that the measurement errors using the CMM fall within the range of [4.5µm – 5.6µm] for an angle variation α in the range of [0°±2.5°; 90°±2.5°].

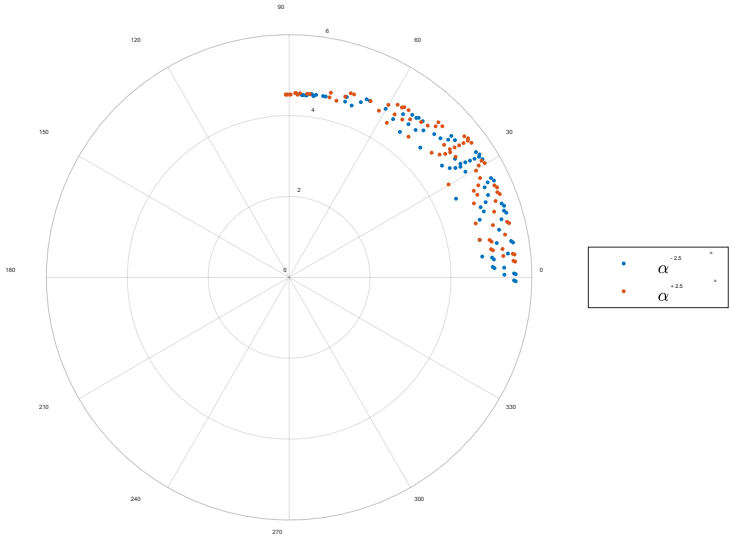

a)

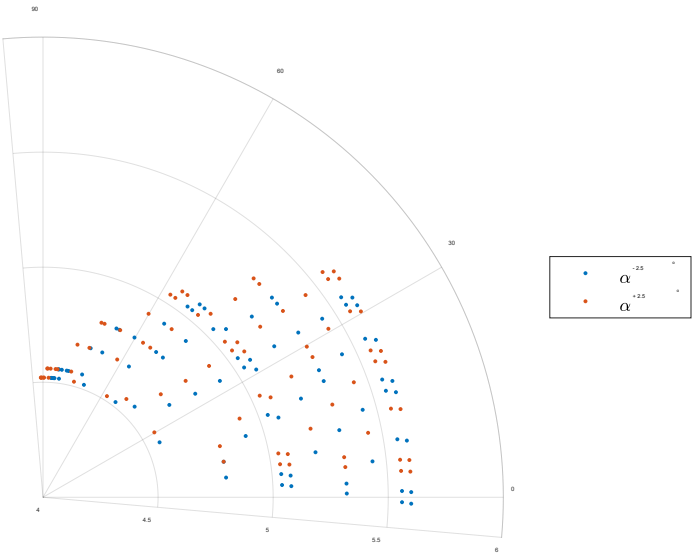

b)

Fig. 5. [X] Polar plot – measurement error distribution (µm) as a function of angle variation (α). **a)** Complete polar plot; **b)** Zoomed-in plot of error distribution. [**14**]

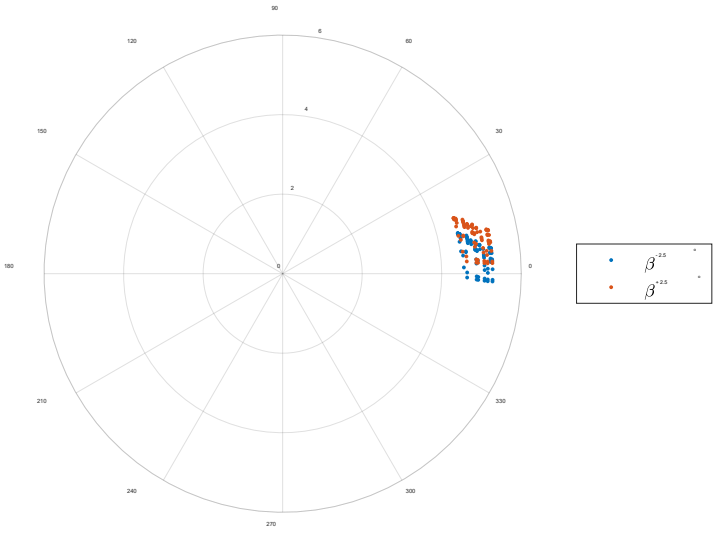

a)

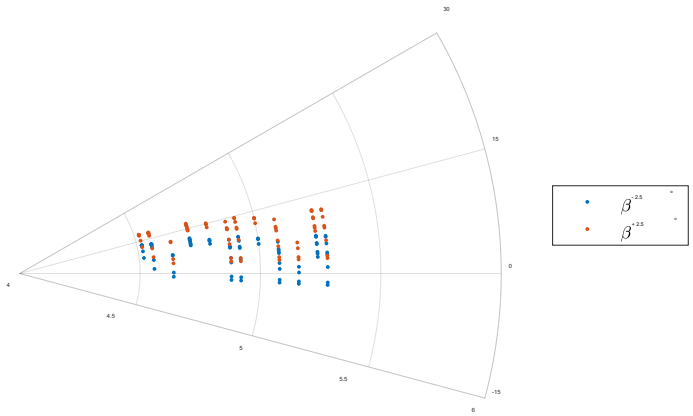

b)

Fig. 6. [Y] Polar plot – measurement error distribution (μm) as a function of angle variation (β). **a)** Complete polar plot; **b)** Zoomed-in plot of error distribution. [**14**]

Analyzing the polar chart in Figure 6, it is observed that the measurement errors using the CMM fall within the range of [4.5μm – 5.3μm] for an angle variation β in the range of [0°±2.5°; 15°±2.5°].

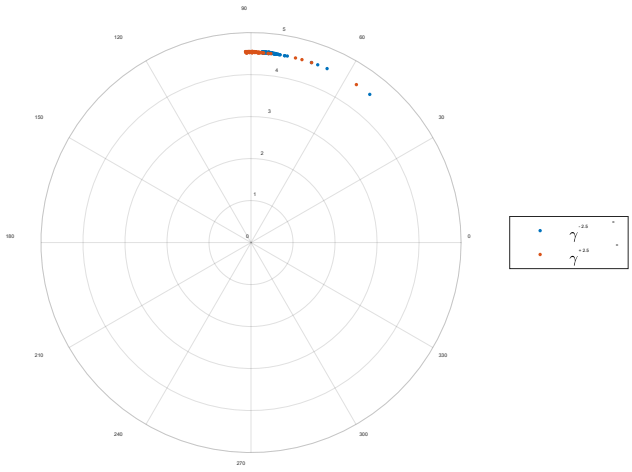

a)

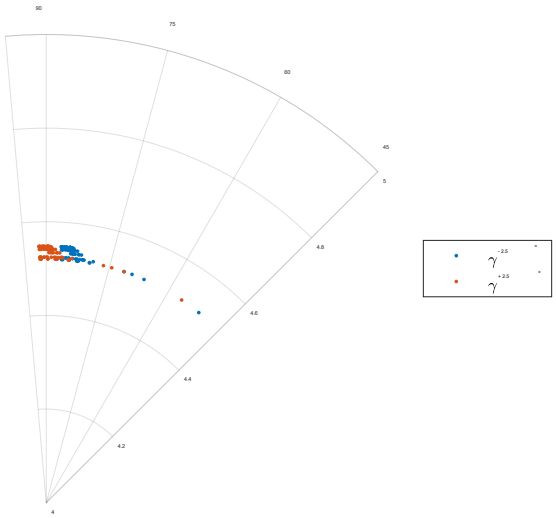

b)

Fig. 7. [Z] Polar plot – measurement error distribution (μm) as a function of angle variation (γ). **a)** Complete polar plot; **b)** Zoomed-in plot of error distribution. [**14**]

Analyzing the polar chart in Figure 7, it is observed that the measurement errors using the CMM fall within the range of [4.5μm – 4.6μm] for an angle variation γ in the range of [50°±2.5°; 90°±2.5°].

Using the data detailed in Table 4 and the mathematical relations 10 – 12, the uncertainty associated with the three directions was calculated in relation to the angles α, β, and γ [**14**]:

$$U_x(\alpha) = \frac{\Delta_{x_{max}} - \Delta_{x_{min}}}{2} = 5,6 - 4,52 = 0,54\mu m \quad (10)$$

$$U_y(\beta) = \frac{\Delta_{y_{max}} - \Delta_{y_{min}}}{2} = 5,28 - 4,52 = 0,38\mu m \quad (11)$$

$$U_z(\gamma) = \frac{\Delta_{z_{max}} - \Delta_{z_{min}}}{2} = 4,55 - 4,52 = 0,015\mu m \quad (12)$$

Next, the measurement uncertainty $U(\alpha,\ \beta,\ \gamma)$ is calculated in relation to the three angles using the relation 13 [**14**]:

$$U(\alpha,\beta,\gamma) = \max\left(U_x(\alpha), U_y(\beta), U_z(\gamma)\right) = 0,54\mu m \quad (13)$$

The total measurement uncertainty of the CMM equipment is calculated using the relation 14 [**14**]:

$$U = \sqrt{U_x^2 + U_y^2 + U_x^2} = 0,66\mu m \quad (14)$$

The measurement uncertainty of the CMM equipment is determined as:

$$U\ =\ 0.66\ \mu m \quad (15)$$

3. Conclusions

$$[U_{computed} = 0.66\ \mu m] > [U_{certificate} = 0.5\ \mu m] \quad (16)$$

One can notice that the computed value of the uncertainty is only slightly increasing by 0.16 μm. However, the percentual increase of the computed uncertainty is 32% bigger than the certificate value, which is a substantial difference.

Based on this finding, the most substantial conclusion concerns the use of CMM for geometrical data of parts and assemblies, particularly in cases where high-precision measurement is required:

a) Researchers and engineers will rely on the equipment calibration certificate as the equipment reference baseline, but can further improve the accuracy of their geometry assessment by employing the described method to evaluate measurement uncertainty for specific specimens, as this is dependent on the distances (X,Y,Z) that the equipment probe needs to travel for each measured point.

Furthermore, distinct precautionary actions are required to influence measurement uncertainty as little as possible.

b) Temperature and humidity variations need to be avoided by installing the CMM equipment in carefully controlled environments. Additionally, when measuring activities that extend for longer periods, it is highly recommended to perform CMM in identical time intervals of the working day.

c) The insufficient sampling rate is one key element that hampers accurate CMM. This is usually driven by budget and resource limitations. It is strongly

recommended that researchers plan sufficient sampling rates during the design of the experiment phase.
d) The human factor influence can be controlled by performing the work with highly skilled and trained personnel (ISO 10360 certification is often mandatory), but also by assigning distinct work packages to a single technician and avoiding the subsequent assignment of several technicians for a single work package.
e) The changes in the support of measured specimens should be avoided throughout the entire CMM process.
f) Intrinsic factors of the CMM equipment can be minimized through the execution of the periodical equipment maintenance as recommended by the manufacturer.
g) Algorithm-induced factors – we recommend the careful employment of software tools used for filtering the results or post-processing, such as surface smoothing.

REFERENCES

[1] *Clean Sky 2 ELADINE Project* under the H2020 Frame Program. Available online: https://eladine-project.eu/ (accessed on 28th of *M*ay 2025).
[2] *Clean Sky 2 OPTICOMS Project* under the H2020 Frame Program. Available online: https://opticoms-horizon2020.com/ (accessed on 28th of *M*ay 2025).
[3] JCGM 100 series – Guides to the expression of uncertainty in measurement (GUM series). JCGM 100:2008 - Evaluation of measurement data. Document produced by Working Group 1 of the Joint Committee for Guides in Metrology (JCGM/WG 1).
[4] *Holman, J.P.* (**2012**). Experimental Methods for Engineers. McGraw-Hill Education.
[5] ISO/IEC Guide 98-3:**2008** - Uncertainty of measurement — Part 3: Guide to the expression of uncertainty in measurement.
[6] *Bendat, J. S., & Piersol, A. G.* (**2010**). Random Data: Analysis and Measurement Procedures. Wiley.
[7] Coleman, H.W., & Steele, W.G. (**2009**). Experimentation, Validation, and Uncertainty Analysis for Engineers. Wiley.
[8] *Taylor, J.R.* (**1997**). An Introduction to Error Analysis: The Study of Uncertainties in Physical Measurements. University Science Books.
[9] *Moffat, R.J.* (**1988**). Describing the Uncertainties in Experimental Results. Experimental Thermal and Fluid Science.
[10] Beckwith, T.G., Marangoni, R.D., & Lienhard, J.H. (**2007**). Mechanical Measurements. Pearson.
[11] *R.G. Easterling, M.E. Johnson, T.R. Bement, and C.J. Nachtsheim*, Absolute and Other Tolerances, SAND88-0724, LA-UR 88-906 (Sandia National Laboratories) **1989**.
[12] VDWDE 2617 Accuracy of Coordinate Measuring Machines (1986), Beuth Verlag, D-1000 Berlin, Germany.
[13] Laboratorul de Metrologie Hexagon Manufacturing Intelligence Romania. Calibration Certificate 309/2024 Serial No. GLOF000384IA; Calibration mark RENAR LE 049.
[14] *C. Banu,* Dual Numerical-Experimental Investigations Regarding the Prediction of Geometric Distortions Induced by Residual Stresses Generated During the Fabrication of Multilayered Anisotropic Structures, Ph.D. Thesis (Released and published for public review at: https://rei.gov.ro/), (**2025**), Bucharest